

# We are IntechOpen, the world's leading publisher of Open Access books Built by scientists, for scientists

6,900

Open access books available

186,000

International authors and editors

200M

Downloads

Our authors are among the

154

Countries delivered to

TOP 1%

most cited scientists

12.2%

Contributors from top 500 universities



WEB OF SCIENCE™

Selection of our books indexed in the Book Citation Index  
in Web of Science™ Core Collection (BKCI)

Interested in publishing with us?  
Contact [book.department@intechopen.com](mailto:book.department@intechopen.com)

Numbers displayed above are based on latest data collected.  
For more information visit [www.intechopen.com](http://www.intechopen.com)



# The Impact of Virtual Environments for Future Electric Powered-Mobility Development Using Human-in-the-Loop: Part A - Fundamental Design and Modelling

*Jun Jie Chong, Peter J. Kay and Wei-Chin Chang*

## Abstract

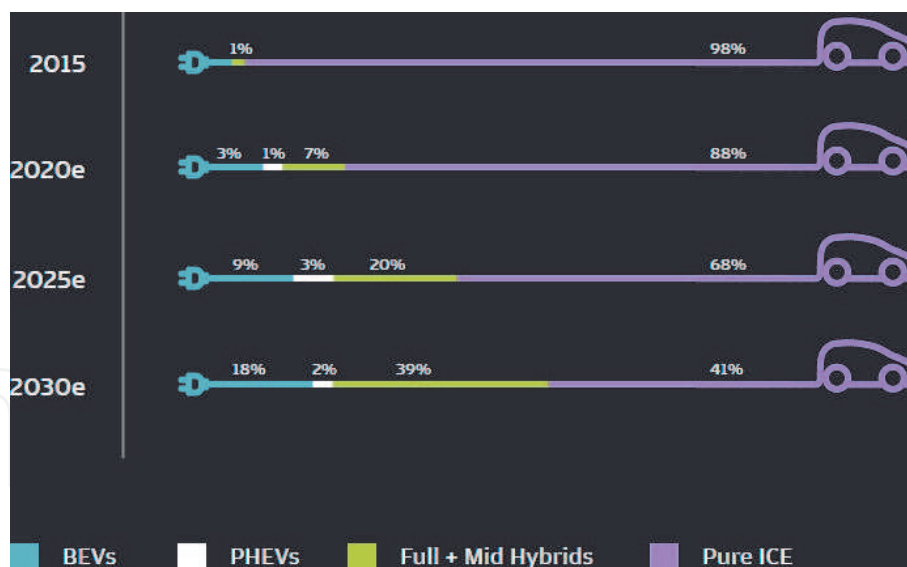
The use of virtual tools will be discussed across two complimentary chapters, Part A explores the fundamental concepts of electric vehicle systems modelling and a design procedure for human-in-the-loop virtual environments; Part B demonstrates how this architecture can be applied to assess energy optimization strategies. In Part A, this research investigates the design and implementation of simulation tools used to predict the energy consumption and strategic tool for the development of an electric vehicle. The case study used is an electric prototype race car for Ene-1 GP SUZUKA competition. Engineering effort is re-directed from physical product design, optimisation and validation to digital tools, processes and virtual testing. This virtual platform is characterised by the integration of two different simulation models—mathematical model of the electric vehicle systems represented by Matlab/Simulink, which accounts for the representation of the powertrain performance prediction that taking into account the resistance motion; and a virtual environment represented by Cruden Software, which accounts recreate topography of real world environment in a driving simulator and incorporate human driver behaviour.

**Keywords:** virtual environment, e-mobility, electric vehicle, virtual testing, Ene-1 GP

## 1. Introduction

Road transportation is one of the largest sources of greenhouse gases (GHG), responsible for climate change, and toxic emissions, responsible for poor human health. In many countries, the zero tailpipe emissions of electric vehicles (EVs) have gained attention from governments as emerging of state-of-the-art technology to reduce emissions from urban transport and improve air quality.

Morgan has carried out a research on global electric vehicle (EV) forecast (**Figure 1**) [1], the report indicates that the electric vehicles and hybrid electric



**Figure 1.**  
Global electric vehicle forecast (source: Morgan estimates) [1].

vehicles (HEVs) is growing and by 2025, EVs and HEVs will account for an estimated 30% of all vehicle sales. It is also evident that, automotive manufacturers are preparing to phase out the internal combustion engine (ICE) vehicles and significantly investing in EVs to capitalise on their growth.

To assist this growth and facilitate the transition from conventional ICE vehicles towards full electrically driven vehicles, the performance (range, efficiency, and etc.) of EVs needs to be improved to mitigate the ‘range anxiety’ of future customers. In order to remain competitive, manufacturers are expected to streamline their new-product-development and manufacturing operations to trim down cost and introduce innovative products will be the most likely to enable them to meet the challenges. Therefore, automotive manufacturers are constantly advancing in new technologies to meet the four key requirements of the market demands, namely: time to market, price, quality, and variety.

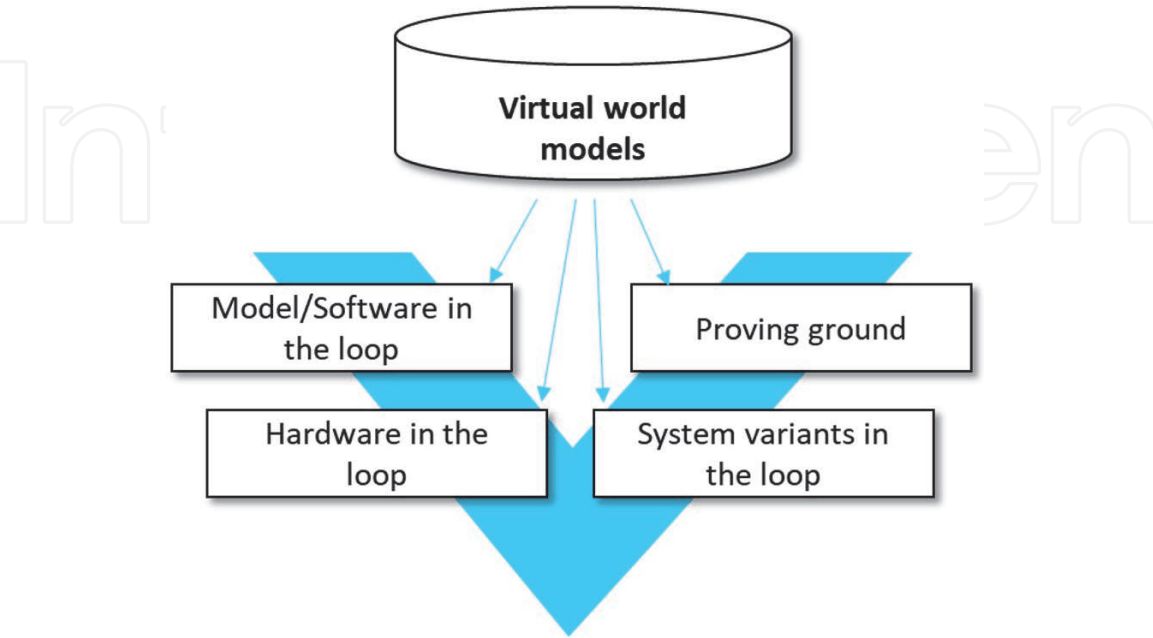
For example, the model-based development methodology has been introduced to the vehicle development route in Ford product development system [2, 3] to enforce the replacement of hardware components by software models in the development process in order to reduce time and cost. Hardware-in-the-loop (HIL) is another important approach regularly implemented in automotive industry to serve as a comprehensive rapid prototyping and automated testing platform. HIL underpins the modelling technique that replaces a physical model, such as an electric vehicle drive train, with a mathematical representation that fully describes the important dynamics of the physical model. Poon et al. [4], highlighted several potential advantages of HIL tools could be beneficial to industrial, enable:

- accelerated testing and validation process;
- reduced testing time needed in the lab;
- caused simulation of all operating points and scenarios that are difficult or impossible to recreate with a real system;
- fault injection capability;
- real-time access to all signals that are difficult to measure in a real system.

In addition to industrial applications, HIL also significantly contribute in the development of Advanced driver-assistance systems (ADAS). For example, A Robust Yaw Stability Controller was designed and tested for a road vehicle under a real time HIL testing [5]. The architecture of the HIL setup employed in that study included, the full-vehicle model ran on a dSpace DS 1103 simulator system, a controller was implemented on an xPC Target Box. The communication controller area network (CAN) bus communicate between the controller (xPC Targetbox) and the vehicle (DS 1103). The yaw rate sensor data, the steering input of the driver, and the vehicle speed can be acquired by the controller, and the steering actuation command can be sent to the vehicle dynamics simulator over CAN bus communication system is designed by which Robust Yaw controller performance is evaluated. Similar approach has been carried out by Gietelink et al. [6], developed an advanced driver assistant for cars and trucks using HIL simulation. In addition, the functioning of adaptive cruise control of automobile has been verified by HIL platform [7]. In Ref. [8], the authors developed a model predictive control approach for adaptive cruise control (ACC) systems and tested with HIL using relevant traffic scenarios, including Stop-&-Go.

According to Tang [9], virtual development is one of the technologies which will enable seamless integration of new processes and continuous improvements in automotive manufacturing. As shown in **Figure 2**, virtual environments (or called it as world models) are successfully integrated into the traditional V-shape model to support process development and validation of the design and performance of components and subsystems at each level. This concept has gained it attention over the recent years, Volvo have announced plans to reduce the development time of their vehicles from 42 to 20 months [10] from concept to start-of-production through the increased reliance on virtual tools, decoupled systems development, and common vehicle and powertrain architectures.

However, vehicle functions are becoming increasingly complexity, the main challenge for virtual development is on the integration of all individual sub-systems to recreate identical overall system behaviour in both virtual and under real world conditions. This chapter describes a generalised method for the fundamental design



**Figure 2.**  
*Virtual world models embedded into V-cycle (adapted from AVL).*

and modelling of vehicle system to be used as a plant model for Human-in-the-Loop application. Furthermore, the model was validated by with the real world data collected from the Ene-1 GP SUZUKA competition.

The paper is organised as follows. Section 2 presents the vehicle plant model development simulation. Simulation and results are given in Section 3. Finally, Section 4 summarises and concludes this chapter.

## **2. Fundamental design and modelling**

This chapter focuses on the fundamental design and development of a vehicle model to be integrated as a digital tool in virtual environment for product design, optimisation and validation.

Several assumptions have been made to construct the models underlie this study:

- A simple vehicle longitudinal model in steady-state condition. This model assumes that the tyres are always contact with the road. Additionally, it is assumed that there is no vertical displacement and the effects of body roll or lateral load transfer is neglected.
- The electric machine is coupled with the inverter devoted as a traction system to convert energy from the vehicle's battery in order to power the drivetrain. For the sake of simplicity, the electrical dynamics of the system are not considered, so the requested torque is equal to the delivered torque, assuming that the torque is within the minimum and maximum limits. Efficiency maps are then used to determine the electric power consumed by the electric machine, given the rotational speed of the machine and the torque request.
- As battery thermal management is not implemented in the prototype, for the sake of simplicity, the thermal behavior of the battery is neglected.

Each sub-system of the vehicle plant model is discussed in the following sub-sections.

### **2.1 Design and development of vehicle model**

The high-level strategy for modelling the car motion is as follows:

- Calculate the tractive force from the powertrain (Section 2.1.1)
- Calculate the sum of all the resistive forces acting on the vehicle (Aerodynamic drag, Rolling resistance, Force due to gradient) (Section 2.1.2)
- Calculate the net force acting on the vehicle (Section 2.1.3)
- Calculate the acceleration of the vehicle (Section 2.1.3)
- Determine the velocity and distance of the vehicle from the first and second integral of the acceleration respectively (Section 2.1.3)

To validate the model a non-commercial vehicle was selected. The reference vehicle chosen was an electric prototype race car for Ene-1 GP SUZUKA competition, as shown in **Figure 3**. The competition is a good case study as it encourages the





**Figure 3.**  
*Electric prototype race car for Ene-1 GP SUZUKA competition.*

competitors to build an electric vehicle that is both fast and efficient. The vehicle was designed according to the rules of the competition.

2.1.1 Tractive force

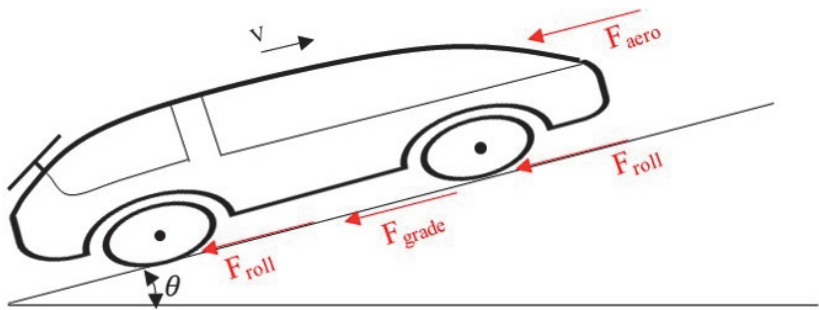
Tractive force is the force produced by the electric machine applied between the tire and road surface to drive a car moving in the longitudinal direction and can be described mathematically as

$$F_{tractive} = \frac{T_t}{r_w} \tag{1}$$

where  $F_{tractive}$  is the tractive force (N),  $T_t$  is the traction torque (Nm) from electric machine,  $r_w$  is the wheel radius (m).

2.1.2 Resistive forces

**Figure 4** shows a generic vehicle travelling up an incline (with inclination angle  $\theta$ ) with the resistive forces acting on the vehicle. The primary aim of this vehicle model is to define the causality between vehicle speed to variations in machine output torque under the different environmental conditions, in which, the propulsion power (from electric machine) has to overcome the retardation forces from the environment to drive the vehicle forward.








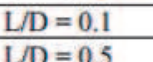



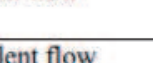
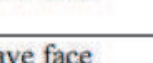
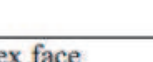

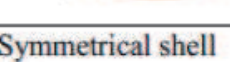

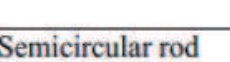




**Figure 4.**  
*Environment forces acting on the vehicle.*

2.1.2.1 Aerodynamic drag force

The aerodynamics drag force mainly consists of two components; shape drag and skin friction. When a vehicle is travelling, there will be a high air pressure zone occurs in front of the vehicle and a low pressure zone appears behind the vehicle, these two zones will result in a resistive force resisting the car from moving forward. The resulting force on the vehicle is the shape drag. The second component of aerodynamic drag force named is as skin friction, is generated due to the fact that two air molecules with different speed create friction. This instance is important in the process of designing a prototype car for the Ene-1 GP SUZUKA competition because aerodynamic losses can account for up to 50% of total energy consumption [11], influence the operating range/speed and eventually affect the competition result. The aerodynamic drag force is defined as:

$$F_{aero} = \frac{1}{2} \rho C_d A (V_x)^2 \tag{2}$$

where  $\rho$  is density of air ( $\text{kg/m}^3$ ),  $C_d$  is aerodynamic drag coefficient, and  $A$  ( $\text{m}^2$ ) is the vehicle frontal area, and  $V_x$  is the speed of the vehicle in longitudinal direction. Depending on the fidelity of the model this can be determined a number of ways. For approximations a value can be taken from **Table 1**, which shows the drag coefficient for a range of standard profiles.

No	Body	Status	Shape	C <sub>D</sub>	
1	Square rod	Sharp corner		2.2	
		Round corner		1.2	
2	Circular rod	Laminar flow		1.2	
		Turbulent flow		0.3	
3	Equilateral triangular rod	Sharp edge face		1.5	
		Flat face		2	
4	Rectangular rod	Sharp corner		L/D = 0.1	1.9
				L/D = 0.5	2.5
				L/D = 3	1.3
		Round front edge		L/D = 0.5	1.2
				L/D = 1	0.9
				L/D = 4	0.7
5	Elliptical rod	Laminar flow		L/D = 2	0.6
				L/D = 8	0.25
		Turbulent flow		L/D = 2	0.2
				L/D = 8	0.1
6	Symmetrical shell	Concave face		2.3	
		Convex face		1.2	
7	Semicircular rod	Concave face		1.2	
		Flat face		1.7	

**Table 1.**  
Drag coefficients for standard profiles.

As it can be seen from the Eq. (2), the aerodynamic force is proportional to the vehicle speed. At constant speeds above 60 km/h, air resistance becomes the dominant retarding force for most vehicles [12]. This source of drag comes from both viscous skin friction as well as form of pressure drag. The form drag caused by the low pressure zone behind the vehicle is dominant factor contributing approximately 90 percent of the total drag [13]. In order to improve reduce the drag resistance, a CFD analysis (**Figure 5**) was performed to evaluate the aerodynamic characteristics of the vehicle and to change the line of its shape and to determine the drag coefficient more accurately.

2.1.2.2 Rolling resistance force

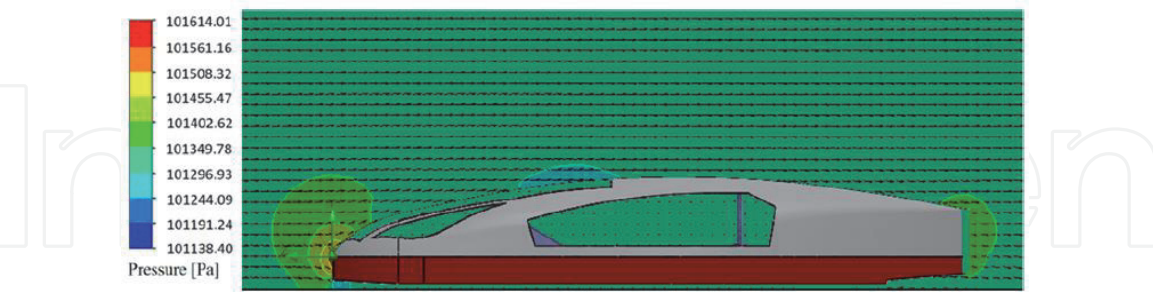
Hysteresis is the phenomenon in which the value of a physical property lags behind changes in the effect causing it. When the tire is rolling, rolling resistance is formed due to the deformation of the tires, Losses occur since the energy required to deform the part of the wheel in contact with the surface is more than that recovered when that part reverts to its original shape. The rolling resistance can be calculated in a simplified manner as a constant depending on the vehicle mass and the rolling resistance coefficient ( $C_{roll}$ ) of the tyres.

$$F_{roll} = C_{roll}mg \tag{3}$$

where  $C_{roll}$  is a coefficient of rolling resistance,  $g$  the gravitational acceleration of  $9.81 \text{ m/s}^2$  and  $m$  (kg) the mass of the vehicle. The rolling resistance coefficients given in **Table 2** are based on experimental results, many empirical formulae have been proposed for calculating the rolling resistance on a hard surface.

2.1.2.3 Gravitational force

As shown in **Figure 6**, the elevation changes act a major challenge for Ene-1 GP SUZUKA competition. The gravitational force is induced by gravity when driving

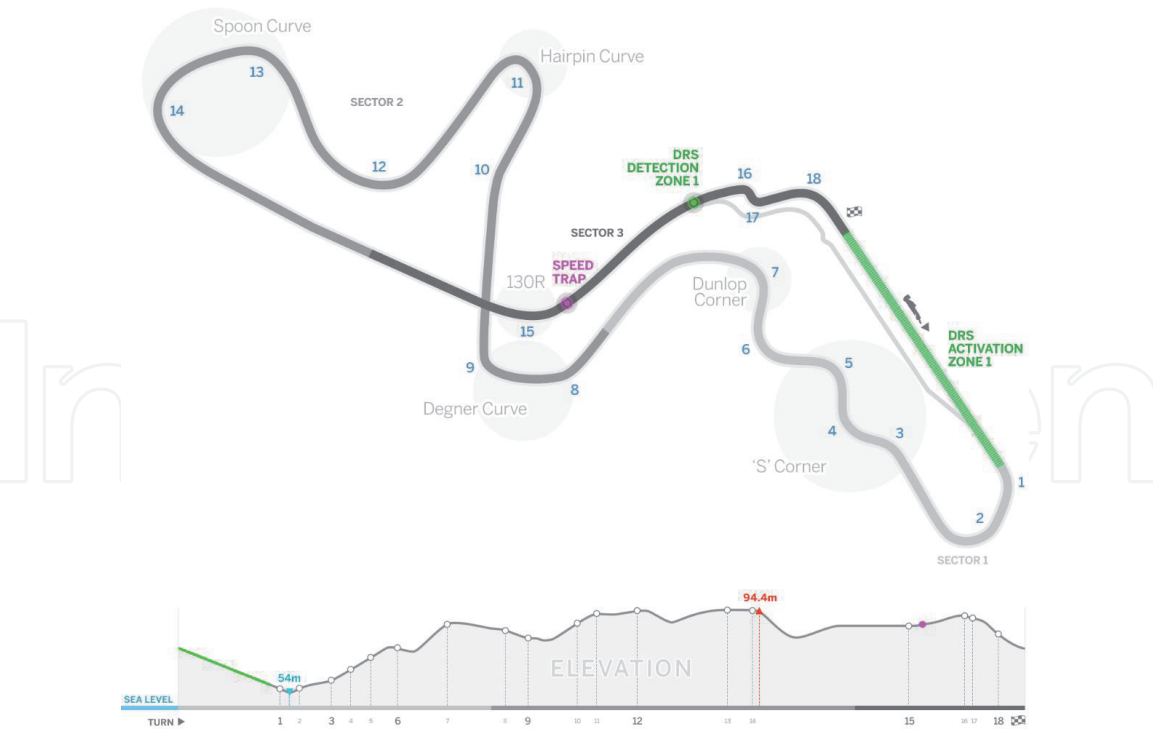


**Figure 5.**  
Sample of the prototype CFD study.

Conditions	Rolling resistance coefficient
Car tires on concrete or asphalt	0.013
Car tires on rolled gravel	0.02
Tar macadam	0.025
Unpaved road	0.05
Field	0.1 - 0.35
Truck tires on concrete or asphalt	0.06 - 0.01
Wheels on rail	0.001 - 0.002

**Table 2.**  
Rolling resistance coefficient at different conditions.





**Figure 6.**  
SUZUKA F1 circuit with elevation profile [14].

on a non-horizontal road and depends on the slope of the road. The force is positive when the vehicle travels on an uphill section and negative on a downhill section. The gravitational force is given by:

$$F_{grade} = mg \sin \theta \tag{4}$$

where,  $g$  the gravitational acceleration of  $9.81 \text{ m/s}^2$ ,  $m$  (kg) is the mass of the vehicle and  $\theta$  (rad) is the inclination angle of the road.

2.1.3 Net force acting on the vehicle

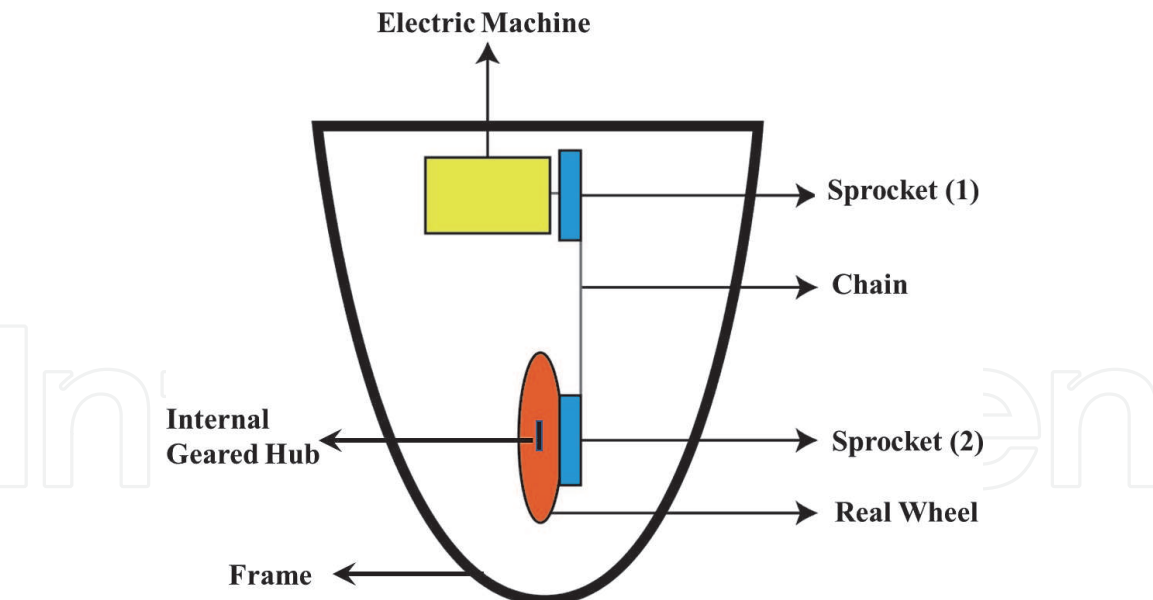
From the Newton’s Second Law of motion, the net force can be described mathematically as

$$F_{tractive} - F_{Resistive} = ma \tag{5}$$

where  $F_{tractive}$  is the tractive force (N),  $F_{Resistive}$  is the total resistive forces (N),  $m$  is the mass of the vehicle (kg),  $a$  is the acceleration of vehicle ( $\text{m/s}^2$ ).

2.2 Design and development of powertrain

The powertrain is a generic model for the components that transfer the torque from the electric machine to the wheels. In this section, it is simplified into an electric machine, transmission (sprockets and chain), and geared hub, all placed according to **Figure 7**. The output shaft of the electric machine is coupled to the sprocket and transmitted to the real wheel by a belt transmission. As shown in **Figure 7**, the internal geared hub is embedded into the real wheel, by using this setup, it will enable the driver has better shifting strategies. Each component has been modelled using a combination of mathematics and lookup tables to accurately capture the behaviour of the system. Specifications of the main components of this powertrain are given in **Table 3**.



**Figure 7.**  
Powertrain system layout.

Component	Specifications
Electric machine	S14502-500R (Tokushudenso)
Sprocket (1)	22
Chain	41.8 mm
Sprocket (2)	90
Internal geared hub	ALFINE SG-S501 (8-speed)

**Table 3.**  
Powertrain system layout.

2.2.1 Electric machine

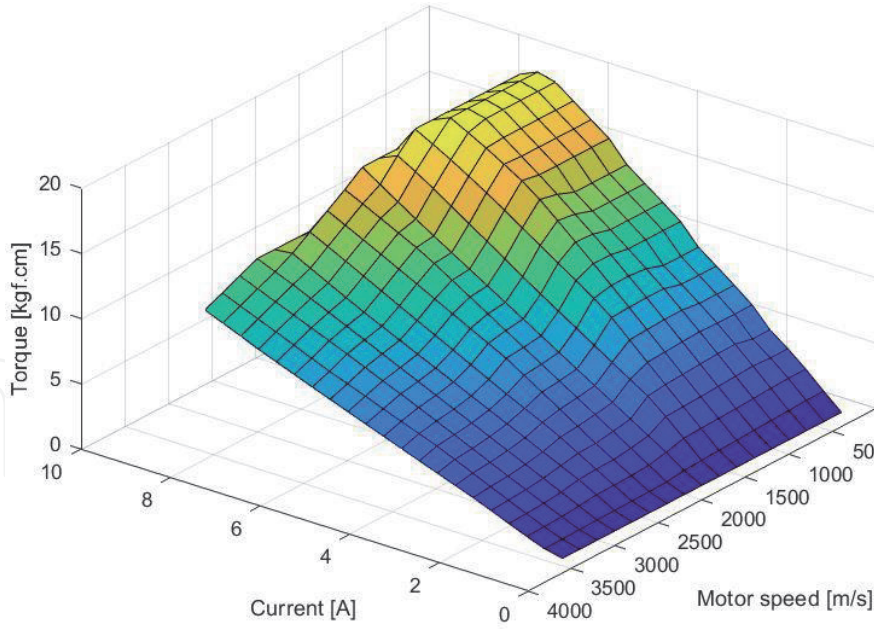
The electric machine model is built using the motor characteristic curve from TOKUSHUDENSO (Japan). The datasets contain sufficient data points to enable a 2D lookup table based performance models to be represented the internal operation of the components. The lookup table is implemented by using the driver demand (A) and electric machine speed (rpm) as inputs and to find the motor torque (N·m) output. A relative torque characteristic plot of the electric machine is shown **Figure 8**.

2.2.2 Driveline

The purpose of the transmissions submodel is to provide maximum vehicle performance and efficiency with wider gear ratios. Detailed ratio design is available in Naunheimer et al. [15] for gradient and speed requirements. Here, the minimum gear ratio for maximum grade climbing is used to evaluate lowest possible ratio, while top speed and driving torque are used to limit the top gear ratio.

$$Gear\ Ratio_{min} \geq \frac{(F_{resistive}) \times r}{n_s \times T_{max}} \tag{6}$$

where,  $F_{resistive}$  (N) is the resistive forces applied on the vehicle,  $r$  (m) is the radius of the wheel,  $n_s$  is the efficiency of the transmission and  $T_{max}$  (Nm) maximum is the



**Figure 8.**  
2D lookup table for electric machine.

electric machine torque. The maximum gear ratio for top speed can be calculated by:

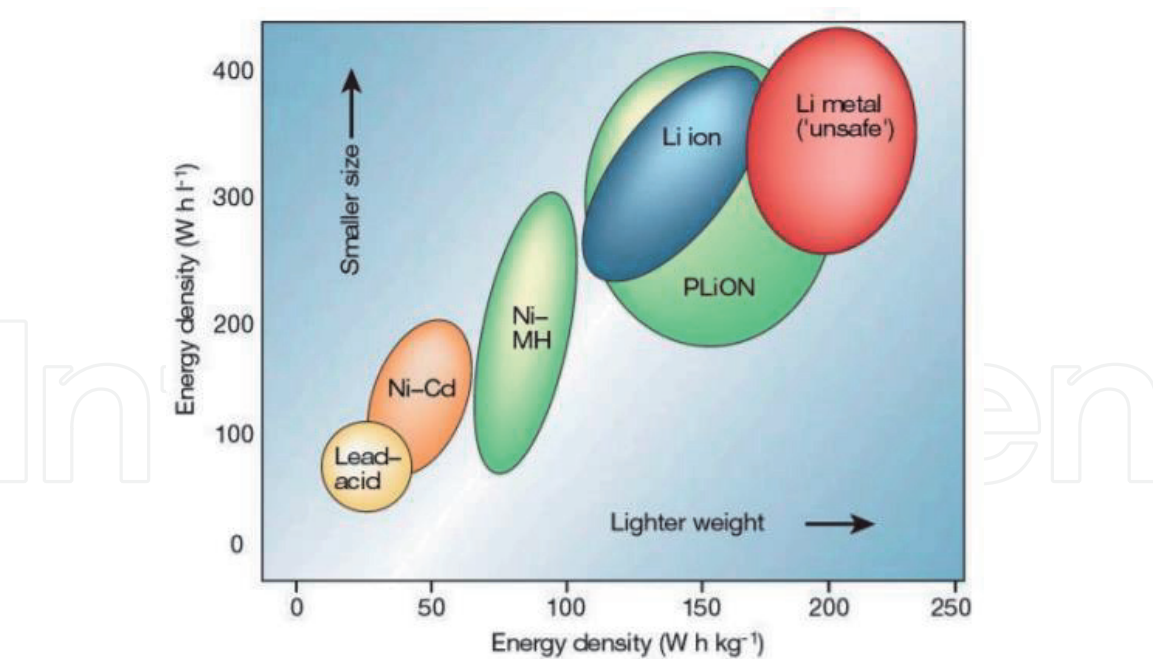
$$Gear\ Ratio_{max} \leq \frac{rpm \times \pi \times r}{30v_x} \quad (7)$$

where,  $v_x$  (m/s) is the vehicle speed in longitudinal direction.

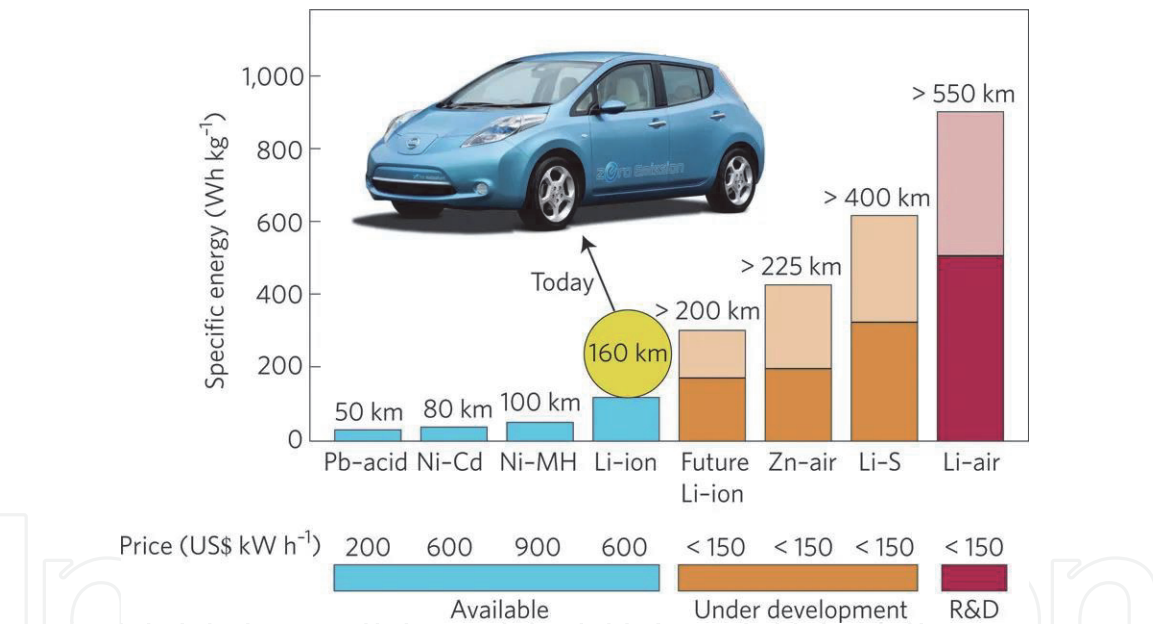
### 2.2.3 Battery model design and development

Energy storages are playing a significant role in today's electric vehicles (EVs) market penetration. Especially, in the realm of battery technologies, manufacturers are aiming to develop a high energy density, flexible and lightweight design for use in most handheld and portable electronics emergence of EVs. The high energy density of Lithium ion batteries (LIBs) have propelled them to become the main choice over the last decade. However, traditional electrode materials (such as commercial lithium cobalt oxide ( $LiCoO_2$ ) cathodes and graphite anodes) have approached their theoretical capacities, limiting the energy density of LIBs ( $\sim 260\text{ W h kg}^{-1}$ ) (**Figure 9**) [18]. Based on the comparison of practical specific energies for several rechargeable batteries presented in **Figure 10** by Bruce et al. [16], Li-S and Li- $O_2$  are amongst the best of rough estimates, because so far there are few realistic prototypes on which to base such figures.

For future battery technologies, the issues of safety and reliability of the battery, accurate information about the state of charge (SOC) and its control still the main challenges. The primary function of the battery system model is to determine the resulting state of charge (SOC) of the battery system from the electrical current demanded from the electrical machine and the. The SOC of the battery is a key measure of performance, since it is directly related to the driving range of the vehicle. The academic literature presents several different battery models. The fidelity of these models differ in terms of the dynamics they represent and the parameterisation requirements they impose to support execution of the simulation. Given the data available to support battery simulation, a simplified steady-state



**Figure 9.**  
Ragone plot of several of the battery technologies used in EVs [18].



**Figure 10.**  
Practical specific energies for some rechargeable batteries, along with estimated driving distances and pack prices [16].

model of the battery has been defined in the form of open circuit voltage (OCV) and cell impedance, both as a function of SOC.

In this competition, under the rules and regulations, the car is powered by Panasonic's AA size EVOLTA nickel metal hydride rechargeable batteries. They are connected 10 in series, forming four pairs. All four pairs are then coupled in series to form a 48 V battery pack. The specifications of the battery can be seen in **Table 4** and additional explanations of the battery setup are described in detail in the competition regulations [17].

To find the OCV dependence of the SOC, experimental was carried at constant current discharge and the result can be seen in **Figure 11**. The state-of-charge and depth-of-discharge depend on the integral of the current drawn or delivered to the battery, and can be calculated by:



$$DoD_{batt} = DoD_{ini} + \int \frac{i_{batt}}{Q_{batt}} dt \tag{8}$$

$$SOC = 1 - DoD_{batt} \tag{9}$$

where  $DoD_{batt}$  is depth-of-discharge,  $DoD_{ini}$  is the initial depth-of-discharge, SOC is the battery state-of-charge,  $i_{batt}$  is the equivalent battery current, and  $Q_{batt}$  is the equivalent battery capacity.

**Figure 12** shows the battery model employed in this study, the battery terminal voltage, as a function of the applied current is:

$$V_{batt} = V_{oc} - I_{batt}R_{int} \tag{10}$$

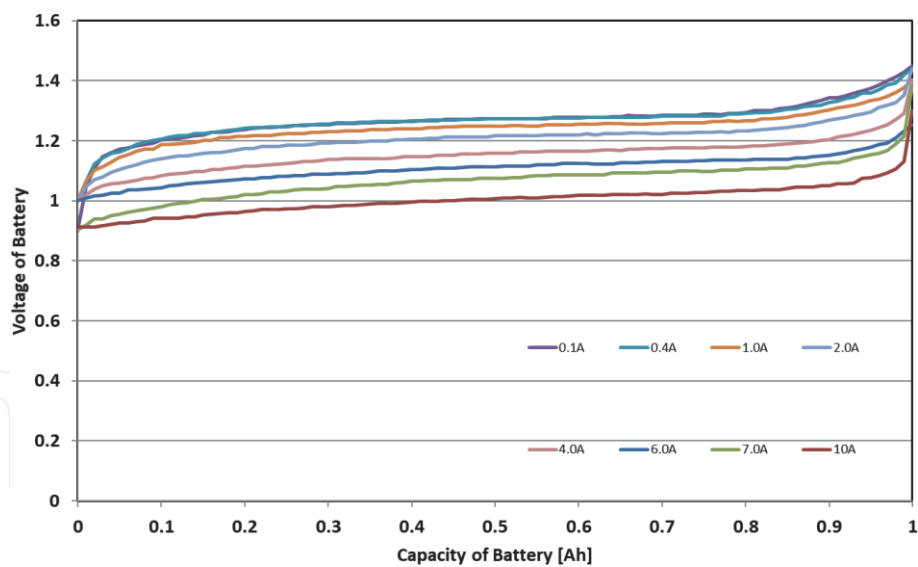
The sign convention employed is: positive current represents current flowing out of the battery, negative current represents current flowing into the battery. Within the context of the complete powertrain model, the value of battery current is directly related to the torque generated by the electrical machine (either through

Type : Nickel-Metal Hydride Battery			Size : AAA Consumer Type
Capacity 1)	Typical		800mAh
	Minimum		750mAh
Nominal Voltage			1.2V
Charging Current x Time		Fast Charge 2)	800 mA x about 1.1h
Ambient Temp.	Charge Condition	Fast Charge 2)	0°C - 40°C
	Discharge Condition		0°C - 50°C
	Storage Condition	Less than 90days	-20°C - 40°C
		Less than 1year	-20°C - 30°C
Internal Impedance 3) (after discharge to E.V.=1.0V)			Approx. 40mΩ (at 1000Hz)
Weight 4)			Approx. 13 g
Size 4) :(Diameter) x (Height)			10.5(D) x 44.5(H) mm

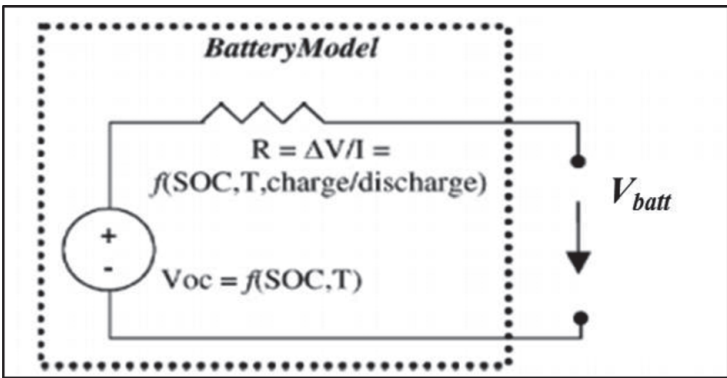
- 1)Single cell capacity under the following condition.  
Charge : 80mA×16h, Discharge : 160mA(E.V.=1.0V) at 20°C
- 2)Use recommended charging system.
- 3)After a few charge and discharge cycles under the above 1) condition.
- 4)With tube.



Table 4.  
Battery Specifications.



**Figure 11.**  
Terminal voltage dependence of different constant discharge currents.



**Figure 12.**  
Battery model employed in this study.

vehicle acceleration or regenerative braking) and any auxiliary load requested by the driver (e.g., vehicle lights etc.).

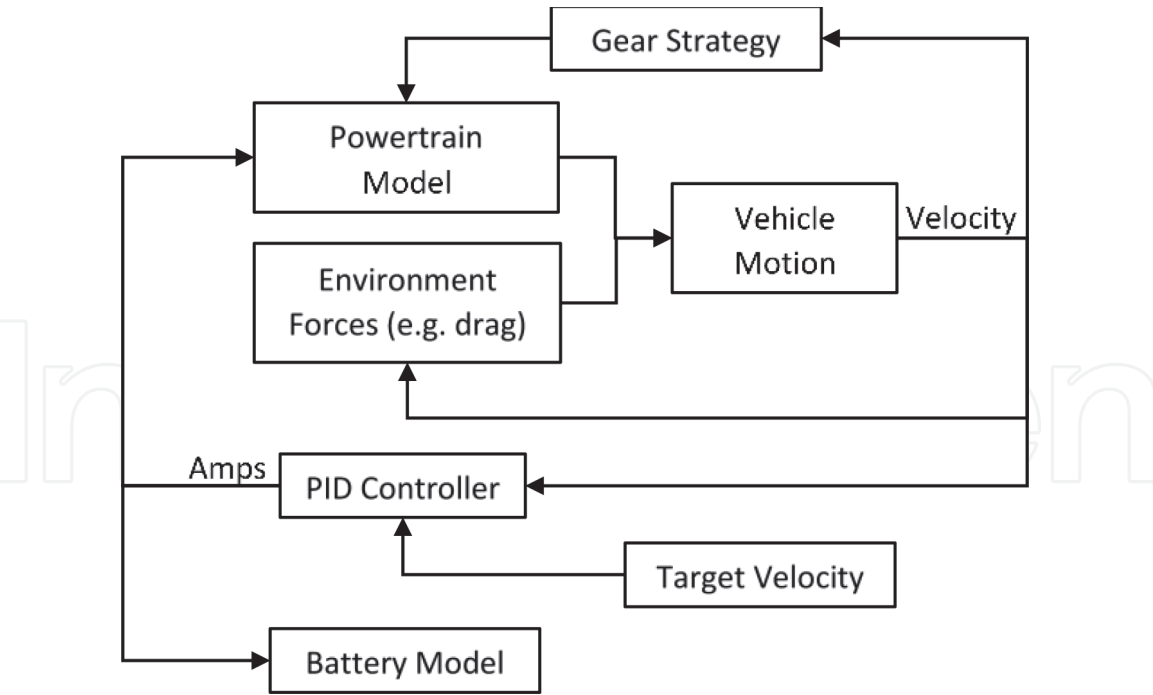
To calculate the battery SOC, the amount of current used during each simulation step is calculated and then subtracted from the initial state of charge at the start of the simulation and is calculated as:

$$SOC = \frac{SOC_{ini} - \int I_{batt} dt}{Ah * 3600} \tag{11}$$

where SOC is the instantaneous state of charge (0–1, 0 is empty and 1 is full),  $SOC_{ini}$  is the initial state of charge (0–1, 0 is empty and 1 is full),  $I_{batt}$  is the charge and discharge current (A) and Ah is the capacity of the battery (Ampere-hour).

### 3. Simulation and results

**Figure 13** shows a summary of how the model is integrated. The target velocity is compared against the actual velocity with the fundamental PID controller. This the demands a current. This current is used to calculate both the torque from the powertrain and the SOC and voltage of the battery. The environmental forces, such as drag, are calculated from the vehicle velocity and position. The environmental forces and the force from the powertrain are used to calculate the vehicle



**Figure 13.**  
*Summary of model integration.*

acceleration, velocity and position. The vehicle (motor) speed is used to determine the gear position from the gear strategy.

The PID controller is based on the proportional, integral and differential gains calculation that can be expressed on Eq. (12), where  $u(t)$  is controlled variable,  $e(t)$  is error value,  $K_p$  is proportional gain,  $K_i$  is integral gain and  $K_d$  is a derivative gain. Then, the PID controller parameters are stated in **Table 5**.

$$u(t) = K_p e(t) + K_i \int_0^t e(\tau) d\tau + K_d \frac{de(t)}{dt} \quad (12)$$

To validate the model simulations were conducted and compared to data collected from the real world from SUZUKA F1 Circuit. **Table 6** presents a representative data-set that can be employed to parameterise the vehicle model and facilitate initial concept simulation studies.

**Figure 14** shows the variation of current with distance travelled for real-world data and simulation. The figure shows that there is broadly a very good agreement between the real-world data and the simulation.

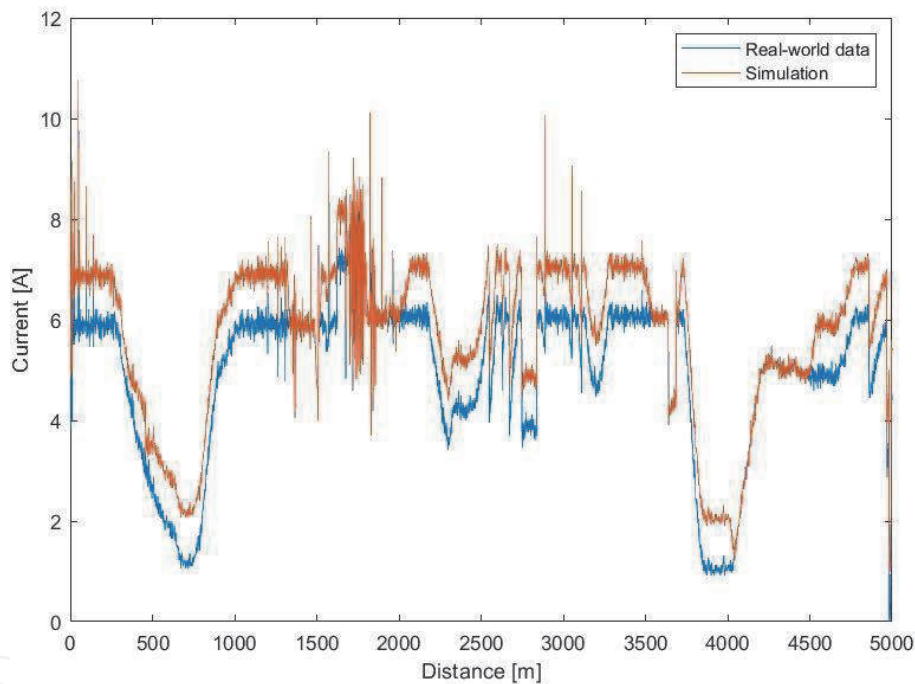
**Figure 15** shows the variation of vehicle velocity with distance travelled for real-world data and simulation. Broadly speaking there is good agreement between the real-world data and the simulation. However, there are some instances where there is some deviation between the real-world data and the simulation, in particular around 1500 m. It is thought that the discrepancy for this is due to the gear shift strategy.

<i>K<sub>p</sub></i>	<b>1</b>
<i>K<sub>i</sub></i>	<b>1</b>
<i>K<sub>d</sub></i>	<b>0</b>

**Table 5.**  
*Fundamental PID controller parameters.*

Parameters	Symbols	Units	Values
Vehicle mass (with driver)	m	kg	77.48
Tyre rolling radius (front, rear)	$R_{wheel\_f}$ $R_{wheel\_r}$	m	0.17
Aerodynamic drag coefficient	$C_d$	—	0.62
Vehicle frontal area	$A_f$	m <sup>2</sup>	0.5
Density of air	$\rho$	kg/m <sup>3</sup>	1.25
Acceleration constant	g	kg/m <sup>2</sup>	9.81
Tyre rolling resistance coefficient	$C_{roll}$	—	0.026
Front track width	tf	m	0.656
Wheelbase	l	m	2.956

**Table 6.**  
Input parameters for vehicle model.



**Figure 14.**  
Variation of current with distance travelled for real-world data and simulation.

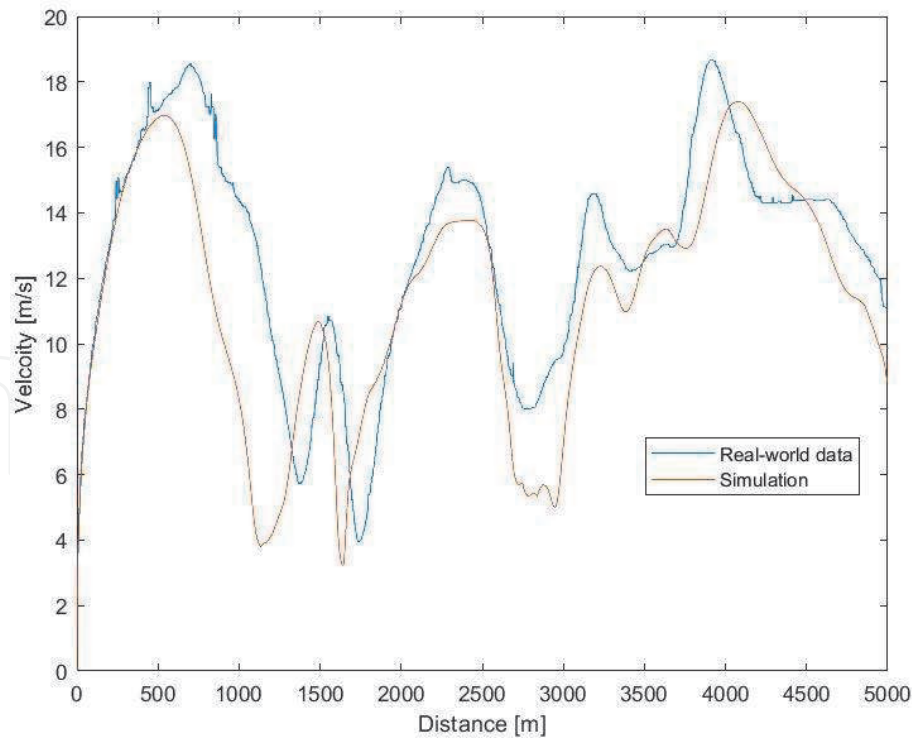
For the real world data the gear that the vehicle was in is not known. Therefore, in the plant model a simple gear strategy algorithm was coded to change gear when the motor speed exceeded 3000 rpm or dropped below 1500 rpm.

However, in real life a human would not change gear based on such a simple strategy. A human would accept the motor speed to temporally increase above the desired threshold if the vehicle was, for example on a steep incline. This will be discussed in the next chapter.

Around 1500 m is where the steepest incline is on the Suzuka circuit. Therefore, it is likely that at this deviation in vehicle velocity is due to the fact that in the real-world the human driver is in an ‘artificially’ low gear to maintain the speed at the steepest part of the circuit.

Taking these factors into account there is reasonable absolute validation of the vehicle model to allow it to be used for future studies.





**Figure 15.**  
Variation of vehicle velocity with distance travelled for real-world data and simulation.

## 4. Conclusion

This chapter presented the development of an electric vehicle model. A real-world non-commercial vehicle was used for validation. The main conclusions are:

- An electric vehicle model has been developed from first principles and commercially available data.
- The results show good absolute validation with real-world data
- The reason for areas where the validation is not as good, is due to the difference between the low fidelity gear strategy used in the model and the gear strategy used by the real-world driver.

IntechOpen

## Author details

Jun Jie Chong<sup>1\*</sup>, Peter J. Kay<sup>2</sup> and Wei-Chin Chang<sup>3</sup>


1 Newcastle University in Singapore, Singapore

2 University of the West of England, Bristol, UK

3 Southern Taiwan University of Science and Technology, Taiwan

\*Address all correspondence to: [junjie.chong@newcastle.ac.uk](mailto:junjie.chong@newcastle.ac.uk)

## IntechOpen

© 2020 The Author(s). Licensee IntechOpen. Distributed under the terms of the Creative Commons Attribution - NonCommercial 4.0 License (<https://creativecommons.org/licenses/by-nc/4.0/>), which permits use, distribution and reproduction for non-commercial purposes, provided the original is properly cited. 

## References

- [1] Morgan JP. Driving into 2025: The Future of Electric Vehicles [Internet]. 2018. Available from: <https://www.jpmorgan.com/global/research/electric-vehicles> [Accessed: 03 December 2019]
- [2] Liker JK, Morgan J. Lean product development as a system: A case study of body and stamping development at ford. *Engineering Management Journal*. 2011;**23**(1):16-28. DOI: 10.1080/10429247.2011.11431884
- [3] Majumder A. Strategic metrics for product development at Ford Motor Company [Thesis]. Massachusetts: Massachusetts Institute of Technology; 2000
- [4] Poon JJ, Kinsy MA, Pallo NA, Devadas S, Celanovic IL. Hardware-in-the-loop testing for electric vehicle drive applications. In: 2012 Twenty-Seventh Annual IEEE Applied Power Electronics Conference and Exposition (APEC); 5-9 February 2012; Orlando. IEEE; 2012. p. 2576-2582
- [5] Guvenc BA, Guvenc L, Karaman S. Robust yaw stability controller design and hardware-in-the-loop testing for a road vehicle. *IEEE Transactions on Vehicular Technology*. 2008;**58**(2): 555-571. DOI: 10.1109/TVT.2008.925312
- [6] Gietelink O, Ploeg J, De Schutter B, Verhaegen M. Development of advanced driver assistance systems with vehicle hardware-in-the-loop simulations. *Vehicle System Dynamics*. 2006;**44**(7):569-590. DOI: 10.1080/00423110600563338
- [7] Short M, Pont MJ. Assessment of high-integrity embedded automotive control systems using hardware in the loop simulation. *Journal of Systems and Software*. 2008;**81**(7):1163-1183. DOI: 10.1016/j.jss.2007.08.026
- [8] Lee MH, Lee HM, Lee KS, Ha SK, Bae JI, Park JH, et al. Development of a hardware in the loop simulation system for electric power steering in vehicles. *International Journal of Automotive Technology*. 2011;**12**(5): 733. DOI: 10.1007/s12239-011-0085-x
- [9] Tang H. *Manufacturing System and Process Development for Vehicle Assembly*. Warrendale: SAE International; 2017
- [10] SAE. Volvo's Rapid Strategy Aims at 20-Month Vehicle Development [Internet]; 2014. Available from: <https://www.sae.org/news/2014/10/volvos-rapid-strategy-aims-at-20-month-vehicle-development> [Accessed: 18 April 2019]
- [11] Abo-Serie E, Oran E, Utcu O. Aerodynamics assessment using CFD for a low drag Shell eco-Marathon car. *Journal of Thermal Engineering*. 2017; **3**(6):1527-1536. DOI: 10.18186/journal-of-thermal-engineering.353657
- [12] Schaltz E. Electrical Vehicle Design and Modeling. In: Soylu S, editor. *Electric Vehicles: Modelling and Simulations*. Rijeka: InTech; 2011. p. 1-24. DOI: 10.5772/958
- [13] Sudin MN, Abdullah MA, Shamsuddin SA, Ramli FR, Tahir MM. Review of research on vehicles aerodynamic drag reduction methods. *International Journal of Mechanical and Mechatronics Engineering*. 2014;**14**(02): 37-47. DOI: 10.26776/ijemm.04.01.2019.0
- [14] Suzuka International Racing Course [Internet]. 2019. Available from: <https://www.formula1.com/en/racing/2017/Japan.html> [Accessed: 12 December 2018]
- [15] Naunheimer H, Bertsche B, Ryborz J, Novak W. *Automotive Transmissions: Fundamentals, Selection, Design and Application*. 2nd ed. Heidelberg: Springer Science & Business Media; 2010. 717 p. DOI: 10.1007/978-3-642-16214-5

[16] Tarascon JM, Armand M. Issues and challenges facing rechargeable lithium batteries. *Nature*. 2001;**414**:359-367. DOI: 10.1038/35104644

[17] Bruce P, Freunberger S, Hardwick L, et al. Li-O<sub>2</sub> and Li-S batteries with high energy storage. *Nature Materials*. 2012;**11**:19-29. DOI: 10.1038/nmat3191

[18] Suzuka Circuit [Internet]. 2019. Available from: [https://www.suzukacircuit.jp/ene1gp\\_s/](https://www.suzukacircuit.jp/ene1gp_s/) [Accessed: 10 February 2019]